KeAi

CHINESE ROOTS
GLOBAL IMPACT

Contents lists available at ScienceDirect

Petroleum Science

journal homepage: www.keaipublishing.com/en/journals/petroleum-science



Original Paper

Pressure control method and device innovative design for deep oil insitu exploration and coring



Nian-Han Wu ^a, Ming-Zhong Gao ^{b, c, *}, Liang-Yu Zhu ^d, Jia-Nan Li ^a, Dong Fan ^e, Bin You ^f, Wei Luo ^g, Guo-Dong Zhu ^e

- ^a School of Mechanical Engineering, Sichuan University, Chengdu, 610065, China
- ^b State Key Laboratory of Hydraulics and Mountain River Engineering, College of Water Resource and Hydropower, Sichuan University, Chengdu, Sichuan 610065, China
- ^c Guangdong Provincial Key Laboratory of Deep Earth Sciences and Geothermal Energy Exploitation and Utilization, Institute of Deep Earth Sciences and Green Energy, College of Civil and Transportation Engineering, Shenzhen University, Shenzhen, Guangdong 518061, China
- d State Key Laboratory of Oil and Gas Reservoir Geology and Exploitation, Southwest Petroleum University, Chengdu, Sichuan 610500, China
- ^e Xi'an Research Institute, China Coal Technology & Engineering Group Corp, Xi'an, Shaanxi 710077, China
- f Haiwang Mechanical Electronic Engineering Technology Co., LTD, Wuhan, Hubei 430064, China
- g Zaoshenzhuang Village, Hancheng Towu, Lubei District, Tangshan, Hebei 064002, China

ARTICLE INFO

Article history: Received 16 May 2022 Received in revised form 17 October 2022 Available online 22 October 2022

Edited by Xiu-Qiu Peng

Keywords:
Deep oil exploration
Fidelity coring device
Temperature-pressure coupling control theory
Pressure control algorithm
Temperature-pressure field alternating model

ABSTRACT

Deep oil exploration coring technology cannot accurately maintain the in-situ pressure and temperature of samples, which leads to a distortion of deep oil and gas resource reserve evaluations based on conventional cores and cannot guide the development of deep oil and gas resources on Earth. The fundamental reason is the lack of temperature and pressure control in in-situ coring environments. In this paper, a pressure control method of a coring device is studied. The theory and method of deep intelligent temperature-pressure coupling control are innovatively proposed, and a multifield coupling dynamic sealing model is established. The optimal cardinality three term PID (Proportional-Integral-Differential) intelligent control algorithm of pressure system is developed. The temperature-pressure characteristic of the gas-liquid two-phase cavity is analyzed, and the pressure intelligent control is carried out based on three term PID control algorithms. An in-situ condition-preserved coring (ICP-Coring) device is developed, and an intelligent control system for the temperature and pressure of the coring device is designed and verified by experiments. The results show that the temperature-pressure coupling control system can effectively realize stable sealing under temperature-pressure fields of 140 MPa and 150 °C. The temperature-pressure coupling control method can accurately realize a constant pressure inside the coring device. The maximum working pressure is 140 MPa, and the effective pressure compensation range is 20 MPa. The numerical simulation experiment of pressure system control algorithm is carried out, and the optimal cardinality and three term coefficients are obtained. The pressure steady-state error is less than 0.01%. The method of temperature-pressure coupling control has guiding significance for coring device research, and is also the basis for temperature-pressure decoupling control in ICP-Coring. © 2023 The Authors. Publishing services by Elsevier B.V. on behalf of KeAi Communications Co. Ltd. This is an open access article under the CC BY-NC-ND license (http://creativecommons.org/licenses/by-nc-nd/ 4.0/).

1. Introduction

Continuous exploitation during the past century has led to the gradual depletion of shallow resources on Earth (Xie et al., 2015), so

E-mail address: gmzh@scu.edu.cn (M.-Z. Gao).

the development of deep oil and gas resources has become a strategic demand for various countries (Gao et al., 2021a). However, the lack of a deep earth exploitation theory makes the exploration of "deep oil" and "deep gas" difficult (Gao et al., 2019). The temperature-pressure characteristics and physical and mechanical behaviors have been distorted, which leads to the distortion of deep theories (Xie, 2017, 2019; Yang et al., 2007; Gao et al., 2019). Therefore, the accuracy of deep rock mechanics theory is directly determined by the accuracy of maintaining the in-situ

^{*} Corresponding author. State Key Laboratory of Hydraulics and Mountain River Engineering, College of Water Resource and Hydropower, Sichuan University, Chengdu, Sichuan 610065, China.

temperature-pressure of deep rock (Pang et al., 2015). However, existing deep rock coring devices cannot accurately control the insitu temperature and pressure. The fundamental reason is the lack of deep temperature and pressure control means and methods (Xiang et al., 2021; Yang et al., 2021). Coring devices are complex and precise downhole equipment (Ruffine et al., 2021). Due to the limitation of the drilling aperture, the core device is filled with various functional parts. Therefore, it is very difficult to integrate core insulation and pressure-maintaining devices in an extremely limited space (Tanner et al., 2021). The pressure and temperature control measures adopted need to break through the limitations of size and high-temperature and high-pressure environments (Guan et al., 2021).

During the deep coring process, two core parameters, namely, temperature and pressure, determine whether core samples can maintain an in-situ state. As shown in Table 1, many countries worldwide have studied the pressure holding capacity of coring devices (Gao et al., 2022). In the field of deep-sea combustible ice coring, a constant sample pressure is the key to preventing the decomposition of combustible ice. Therefore, most combustible ice coring tools have a certain pressure holding capacity. In 1983, the Ocean Drilling Program (ODP) organization of the United States developed a second-generation pressure core barrel (PCB) coring device, i.e., the pressure core sampler (PCS). The sealing mode of the coring device is a ball valve, and its maximum working pressure is close to 70 MPa (Zhang and Yang, 2009). The device has been used in many field experiments to extract pressure-maintaining combustible ice in the Blake Ridge (Dickens et al., 2000). The hydrate coring equipment system (HYACE), funded by EU marine science and technology projects, has successfully collected pressure-retaining cores, which can be transferred to the measurement system at an approximate in-situ pressure of 35 MPa (Milkov et al., 2004). At present, coring technology can only achieve low-pressure sealing (N.H. Wu et al., 2020), which is far from coring in a deep ultrahigh-pressure environment, and cannot achieve stable pressure control (Gao et al., 2018a, 2018b, 2021b).

As shown in Fig. 1, the deep coring environment is high temperature and high pressure. The specific requirements for the control algorithm in this environment are small memory, fast response and strong stability. The PID control algorithm based on the optimal parameters is an algorithm that meets these three conditions at the same time. At the same time, other algorithms either have too much memory or have slow response speed and cannot meet the requirements.

Pressure control involves a wide range of technologies and applications, and many fields have higher requirements for it. Scholar Yang proposed a positive-negative servo system in the field of air pressure control to realize the dynamic adjustment of seal chamber pressure (Yang et al., 2017). The fuzzy PID control algorithm is used to realize the control in the range of 2—140kpa. However, its control core component is the valve system, which is too large and cannot be used under the condition of limited internal space of the coring device. In the field of chemical industry, in order to control the pressure in the distillation tower, Scholar Stefano used the integral

Table 1Acronyms and full names.

Acronym	Full English name
PID	Proportional- Integral- Differential
ICP-Coring	In-situ condition-preserved coring
ODP	Ocean Drilling Program
PCB	Pressure core barrel
PCS	Pressure core sampler
PTCS	Pressure and temperature coring system

absolute error as the parameter variable to reduce the disturbance in the control process (Ciannella et al., 2018). It was proved superior to the traditional pressure control scheme. The control theory of this method was innovative. However, in the multi-field coupling environment, the control system is not clear and impossible to select and evaluate the effective range of integration error in advance. The control object in his study was a large distillation column. The control method was solenoid valve circuit control. The pressure compensation depended on the pressure pump and cannot be applied to the accurate control of small space. In the research of pressure pump control, scholar Li adopted the dualmode variable control method (Li et al., 2020), which effectively improved the control effect of pressure pump. The control object of this method was pressure pump, which had large volume and have no downhole service conditions (Gao et al., 2021c).

As mentioned above, compared with a single pressure field, multiple physical fields interfere with each other in the coring environment (Gao et al., 2021d, 2021e). Therefore, as the control object, the control model of the pressure system has great uncertainty, and the ordinary negative feedback control method cannot be used. At the same time, the current pressure control methods are mostly valve control and pump compensation, which cannot be applied to narrow coring devices. Thus, the fundamental reason why fidelity coring pressure cannot be controlled at present is the lack of effective pressure control theory and method. The core difficulties include deep control system integration, control structure miniaturization and control mean breakthrough.

Although many countries in the world were concerned about coring in pressure environment. However, there were no researches on pressure control methods for deep coring environment at present, and only a few studies have done work on sealed and pressure maintaining coring, so they do not have the ability of pressure control. Therefore, this paper purposed to propose a pressure control method suitable for deep coring environment, which was verified by simulation and experiment. In this paper, the pressure precision control of deep fidelity coring is studied, the temperature-pressure coupling alternating theory in the deep coring environment of the earth is constructed, and a multifield coupling dynamic sealing model is established, the optimal cardinality three term PID intelligent control algorithm of pressure system is developed. The intelligent temperature and pressure control system of the coring device is developed and verified by experiments.

2. Temperature and pressure alternating control theory and sealing model of the coring device

2.1. Temperature and pressure alternating control model of the coring device

The core function of the deep in-situ fidelity coring tool is to keep the core temperature and pressure unchanged. The deep coring process uses a hydraulic screw motor to drive drilling (Alali et al., 2021), so the core enters the pressure holding chamber and is in an environment of liquid intrusion. The pressure holding chamber is filled with water when it is closed (Gao et al., 2020).

Due to the low compressibility of water, the pressure in the pressure chamber will decrease rapidly in the case of seal leakage in the pressure chamber (Ding et al., 2021). Therefore, this paper proposes a pressure compensation method for gas-compatible cavities. Under the condition that the pressure balance between the gas-compatible cavity and the liquid-compatible cavity is achieved, the pressure is controlled by the gas-compatible cavity.

As shown in Fig. 2, after the coring device completes the coring operation, the center rod grabs the core and pulls it into the core

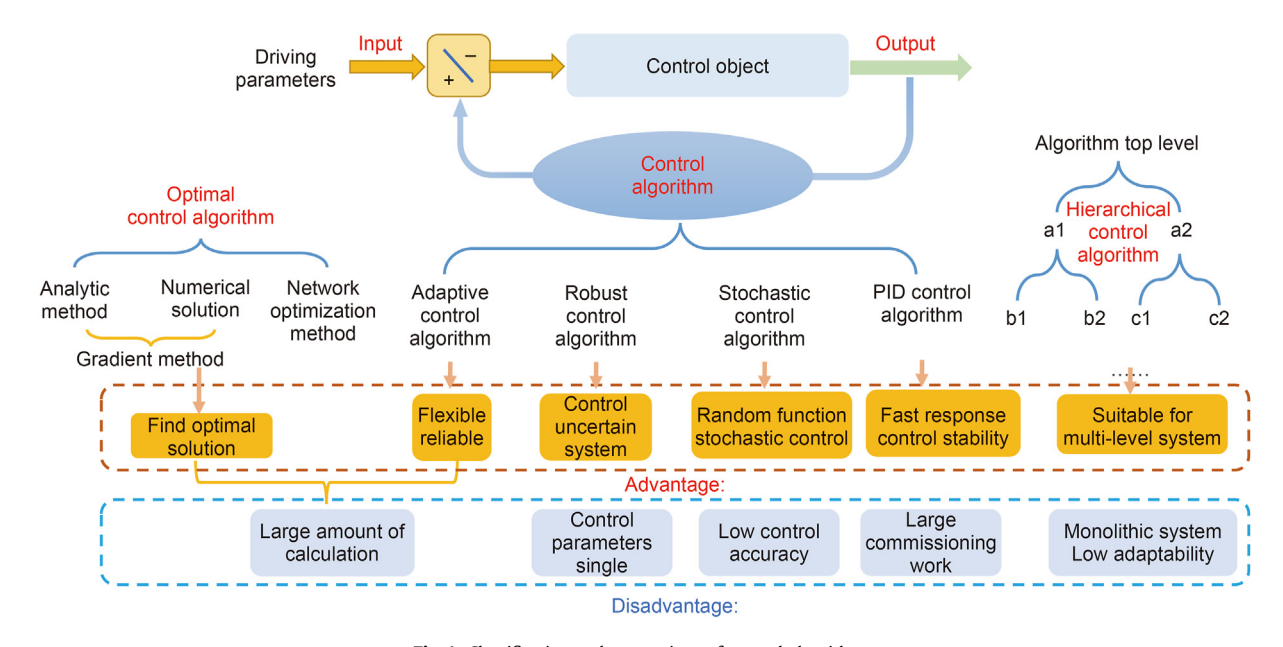


Fig. 1. Classification and comparison of control algorithms.

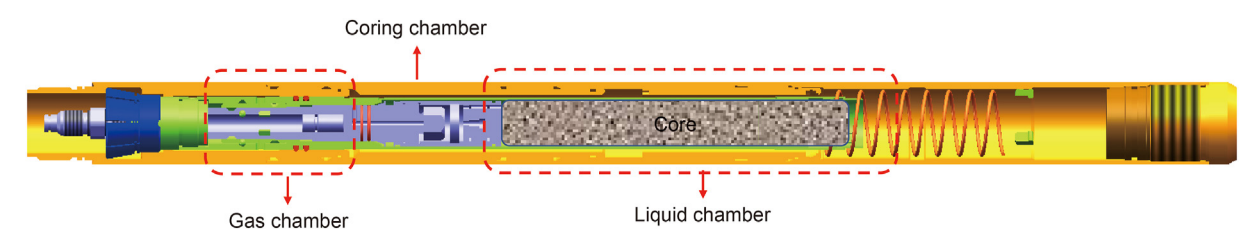


Fig. 2. Schematic diagram of the internal structure of the coring device.

chamber, and along with the core entering the core chamber, there is also the in-situ water phase of the core. At this time, the pressure in the core cavity is the same as the in-situ pressure of the core, so the whole core cavity constitutes a sealed high-pressure container filled with liquid and contains multiple high-pressure sealing structures.

There are two kinds of liquid pressure sources for closed high-pressure vessels: elastic expansion of the vessel and compression of the liquid (Lyras et al., 2021). Compared with the coring device, during in-situ coring, the internal and external pressures are balanced, and the volume of the container will not change. Therefore, hydraulic pressure is generated by the compression of in-situ liquid, and the main component of in-situ liquid is water. The variation law of its volume *V* with pressure can be expressed as:

$$V = V_0(1 - \beta(P - P_0)) \tag{1}$$

In the above formula, P_0 is the initial pressure of water, V_0 is the initial volume of water, and β is the compressibility of water, which is related to temperature and pressure (Zhu et al., 2021). f(P,T) is the influencing factor of water temperature and pressure on compressibility. Therefore, the actual compressibility coefficient of water is:

$$\beta(P,T) = \beta_0 f(P,T) \tag{2}$$

The in-situ pressure and temperature of coring reach 140 MPa and 150 °C (Zhang et al., 2021). When the core is lifted to the ground, the ambient pressure is standard atmospheric pressure.

$$P_0 \ll P$$
 (3)

Therefore, the pressure *P* in the pressure holding chamber can be expressed as:

$$\Delta V = \beta(P, T)PV_0 \tag{4}$$

Fluid leakage rate of the liquid-compatible cavity $Q_{L\nu}$ is as follows:

$$Q_{Lv} = \sum_{i=1}^{n} C_{w} f(Q_{Li}, t)$$
 (5)

Considering the pressure change in the holding chamber, the comprehensive leakage rate is as follows:

$$\Delta V - \sum_{i=1}^{n} C_{w} f(Q_{Li}, t) = \beta(P, T) P V_{0}$$
 (6)

$$\Delta V = \sum_{i=1}^{n} C_{W} f(Q_{Li}, t) \tag{7}$$

When Eq. (7) is satisfied, the pressure in the container will become 0:

$$P = 0 (8)$$

Equation (8) shows that when the amount of water leakage is equal to the compressed volume of in-situ formation water, the

pressure in the pressure holding chamber will be reduced to zero.

$$\beta(140, 150) = 4.5 \times 10^{-10} \, p_a \tag{9}$$

When the space volume of the pressure holding chamber of the whole coring device is 3 L, the initial hydraulic shrinkage is as follows:

$$\Delta V = 140 \times 10^6 \times 4.5 \times 10^{-10} \times 3 = 0.189 L \tag{10}$$

According to the above formula, because the water compression coefficient is small and the leakage rate has a great influence on the pressure, it is impossible to realize constant pressure control only by adopting closed pressure-maintaining technology (Tian et al., 2021).

Therefore, to keep the pressure in the coring device constant, this paper innovatively proposes an intelligent temperature-pressure coupling control method based on the gas-liquid pressure balance principle, as shown in the following figure.

As shown in Fig. 3, a high-pressure gas-liquid balancer is integrated in the center rod, and the high-pressure liquid in the core chamber is led to the liquid chamber through the liquid inlet. The balance piston will move toward the gas chamber under hydraulic pressure and squeeze the gas. Eventually, the pressure in the gas chamber P_C will be the same as the pressure in the liquid chamber P_C .

$$P_C = P_L = P_G \tag{11}$$

The filter is a porous network structure, which is used to filter debris, crushed stone, and other impurities in the core cabin liquid. The bursting pressure of bursting disc is 160 MPa. When the downhole pressure increases sharply, to protect the coring device from damage, the bursting disc will be fractured to release pressure.

Under this model, the pressure in the gas chamber satisfies the Clapeyron equation (Takigawa and Horinaka, 2020).

$$P_{g}V_{g} = nRT_{g} \tag{12}$$

The volume of the gas chamber and the volume V_l of the liquid in the pressure holding chamber satisfy:

$$V_g + V_l = V_h \tag{13}$$

 V_b is the sum of the volumes of the whole pressure holding cabin and the pressure control cabin.

The initial gas-compatible cavity volume V_{g0} satisfy:

$$V_{g0} = \frac{nRT_{g0}}{P_l} \tag{14}$$

 ΔV_g is the gas volume variation in the gas-compatible cavity, and ΔV_l is the volume change of liquid in the pressure holding chamber.

 G_g is the gas leakage rate of the gas-compatible cavity, which can be known from the above formula.

$$\Delta V_l = \Delta V_g + G_g \tag{15}$$

The gas-liquid volume equilibrium equation satisfy:

$$\Delta V_{l} = \beta(P, T)(P_{c} - P_{0}) \left[V_{l} - \left(\Delta V_{g} + G_{g} \right) \right] + \sum_{i=1}^{n} C_{w} f(Q_{Li})$$
 (16)

$$\Delta V_g = \frac{\beta(P, T)(P_c - P_0)V_l + \sum_{i=1}^{n} C_w f(Q_{Li})}{[1 - \beta(P, T)(P_c - P_0)]} - G_g$$
(17)

 P_g is the gas pressure of the gas-compatible cavity, and P_l is the liquid pressure in the pressure holding chamber.

$$P_{c} = P_{g} \tag{18}$$

The gas-liquid pressure balance equation is

$$P_{g} = P_{l} = \frac{nRT_{g}}{V_{g0} - \Delta V_{g}} = \frac{\Delta V_{l} - \sum_{i=1}^{n} C_{w} f(Q_{Li}, t)}{\beta(P, T) V_{0}}$$
(19)

According to the above formula, the equation becomes:

$$P_c = P_g = \frac{nRT_g}{V_{g0} - \Delta V_g} \tag{20}$$

During deep coring, the pressure in the holding chamber is much higher than the initial atmospheric pressure, and the original equation changes as follows:

$$P_{c}\left(V_{g0} - \frac{\beta(P, T)V_{l}}{1 - \beta(P, T)} - G_{g}\right) + \frac{\sum_{i=1}^{n} C_{w}f(Q_{Li})}{1 - \beta(P, T)} = nRT_{g}$$
(21)

The relationship between the temperature in the gas compatible cavity and the pressure in the pressure holding chamber is as follows:

$$P_{\mathcal{C}} = AT_{\mathcal{G}} - B \tag{22}$$

$$A = \frac{1 - \beta(P, T)nR}{1 - \beta(P, T)(V_{g0} - G_g) - \beta(P, T)V_l}$$
 (23)

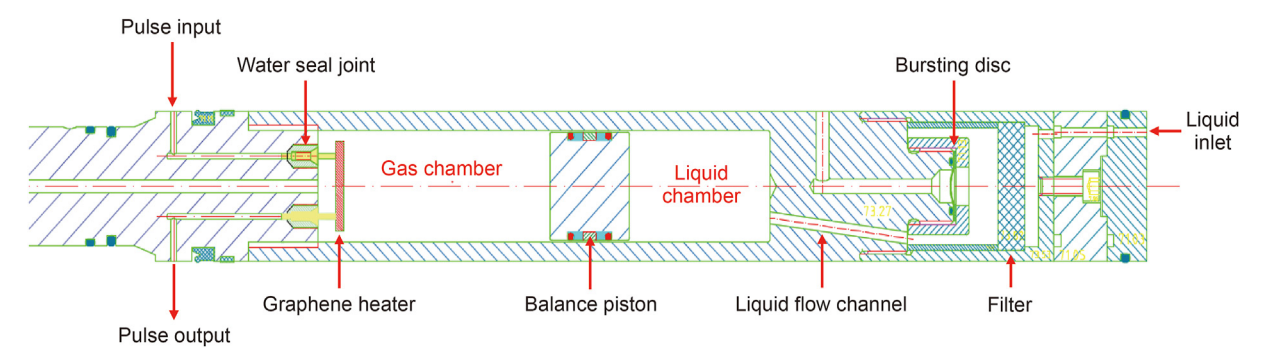


Fig. 3. Intelligent control of pressure based on gas-liquid balance system.

$$B = \frac{1 - \beta(P, T)nR}{\sum_{i=1}^{n} C_{w} f(Q_{Li})}$$
 (24)

The above formula is the pressure-temperature alternating model of the pressure control system of the deep in-situ coring device. An intelligent temperature-pressure coupling control method is proposed based on this theory. The formula shows that the gas temperature in the accumulator is positively correlated with the pressure in the pressure holding chamber, and the pressure in the pressure holding chamber can be controlled by changing the temperature of the gas-compatible chamber. Compensation of the change in pressure value caused by leakage realizes the stability of the pressure value in the pressure chamber.

2.2. Multifield coupling sealing model of the coring device

The pressure chamber of the coring device is a closed chamber for storing the core, and its sealing performance directly determines whether the in-situ pressure environment of the core can be well maintained. The pressure chamber is not a whole but a combination of several sealing models.

The environmental fields involved in the multifield coupling sealing model of the corer include a deep ultrahigh-pressure field, a high-temperature field, a fluid field, a polymer-metal contact field and a mechanical action field. The pressure field acts directly on the sealing surface and exerts shear force on the sealing parts. The high-temperature field is a change field, and the temperature will reduce the viscosity and shear strength of polymer sealing materials (Gao et al., 2021c).

In addition to being a sealed container, the pressure holding chamber contains various parts and structures for coring. To consider the action realization and ultrahigh pressure sealing of the pressure holding chamber, the pressure holding chamber adopts various sealing methods, such as anisotropic curved surface sealing (Pruchnicki et al., 2021), multitube nested sealing, and thread radial sealing. From the sealing mode, the sealing of the pressure holding cabin can be divided into three categories: 1. fixed sealing structure; 2. separate sealing structure inside the coring device; and 3. special sealing valve structure, as shown in Figs. 4-6.

1) Before coring, the fixed seal inside the coring device has achieved the sealing assembly requirements and reached the sealing standard. The fixed seal structure includes a fluoropolymer, i.e., polytetrafluoroethylene (PTFE), rubber retaining ring seal between pipe threads and a seal of thread penetrating parts.

- 2) Before coring, no sealing standard is formed, and the classification of late sealing by the action of the coring device in the working process is a separated sealing structure. The separated seal structure includes a multitube nested seal and a moving radial seal.
- 3) The special sealing valve structure is the structure in which the coring device realizes core passing and high-pressure sealing. It is a self-triggering anisotropic curved surface sealing structure, which exhibits dynamic sealing during the coring process (Lyu et al., 2021).

3. Design of the temperature-pressure coupling control system for the coring device

Based on the temperature-pressure alternating model of the coring device described above, a method to control the pressure of the liquid phase by controlling the temperature of the gas phase was determined. In this paper, the pressure compensation method for the pressure chamber of the coring device is proposed. Based on the approximate positive correlation between the temperature parameters of the gas-compatible chamber and the pressure value in the pressure chamber, an intelligent compensation system for the ultrahigh pressure of the coring device was designed and manufactured. The core of this method is to establish a high-voltage circuit sealing system and an intelligent control system in a small space. Therefore, this method is especially suitable for pressure control in complex temperature-pressure coupling environments, such as deep fidelity coring devices.

As shown in Fig. 7, the ultrahigh-pressure intelligent control system relates to the core holding chamber of the coring device. After the holding chamber enters a sealed state, the in-situ formed water seal is stored in the holding chamber, and the whole holding chamber is a liquid chamber. Therefore, the liquid-compatible cavity communicates with the high-pressure liquid environment in the pressure holding chamber through the liquid inlet, and the obtained fidelity core is stored in the pressure holding chamber. The gas-compatible chamber maintains pressure balance with the liquid chamber through a high-pressure balance piston. Since the leakage of liquid is the main reason for the pressure reduction of the pressure holding chamber, the pressure leakage is compensated by a gas with greater compressibility. To maintain the in-situ pressure of deep rock, the in-situ coring device for deep rock needs to be pressurized. Based on the temperature-pressure alternating model of the coring device pressure control system, the pressure in the coring device pressure chamber can be controlled by changing the temperature of the gas-compatible chamber.

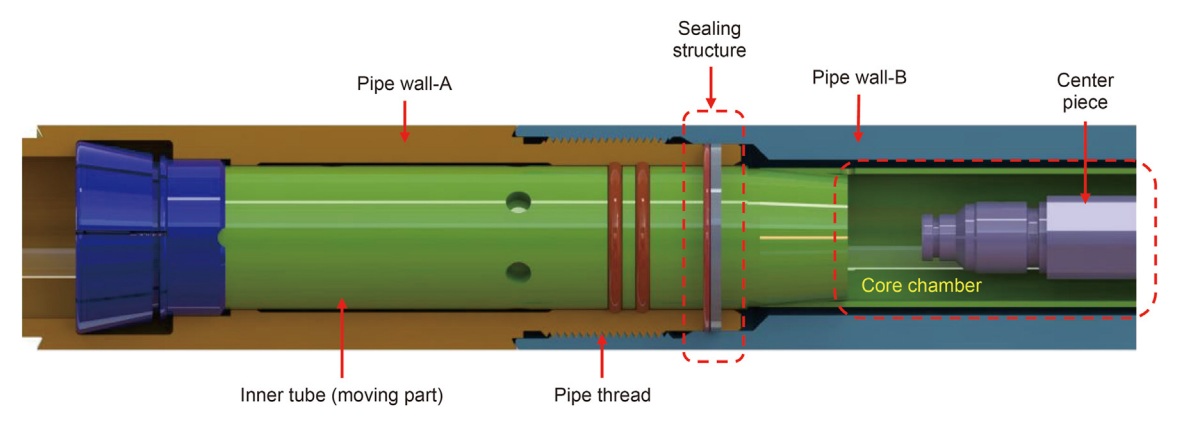


Fig. 4. Fixed sealing model of the coring device.

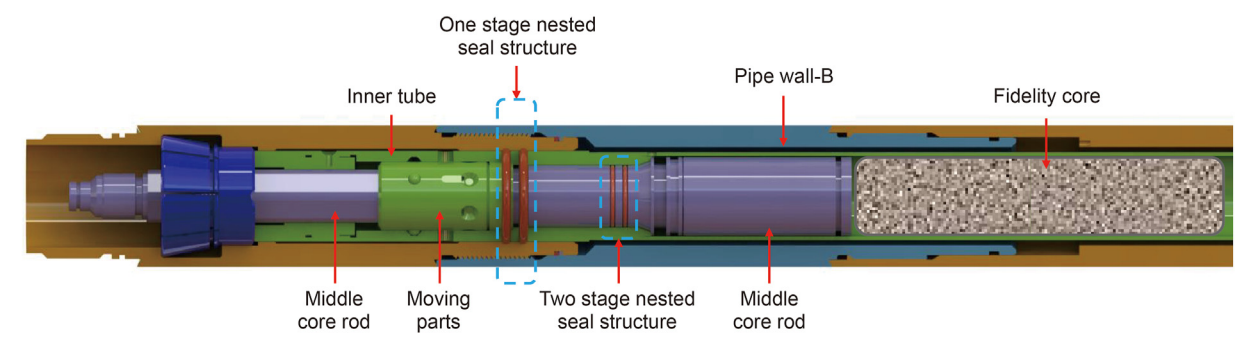


Fig. 5. Separate seal model of the coring device.

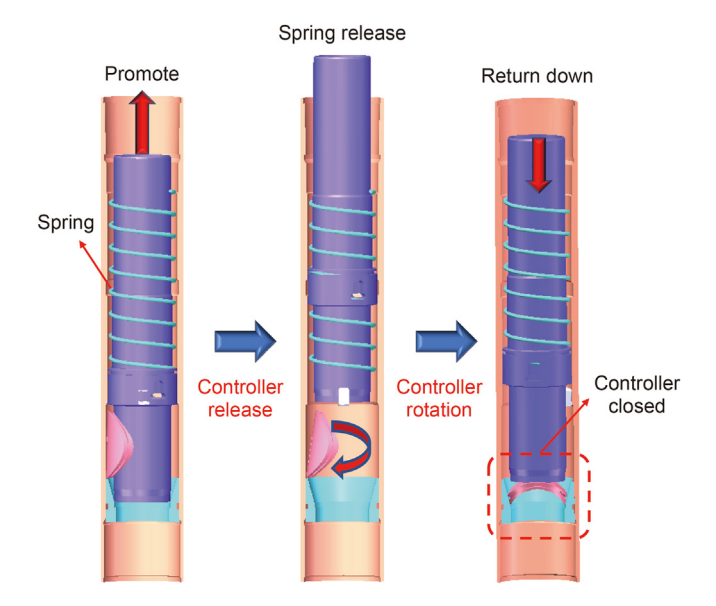


Fig. 6. Special sealing valve model of the coring device.

The control principle of the temperature-pressure alternating control system is shown in Fig. 8. Based on the dynamic balance principle of gas-phase and liquid-phase pressures, using the temperature-pressure coupling characteristics of the gas-compatible cavity, the pressure of the gas phase is controlled by the pulse current power input, and then the pressure of the liquid phase is controlled to solve the problem of pressure compensation in a complex and narrow deep environment. The method and technology are provided for maintaining and controlling the pressure of the coring device. This scheme is based on the negative feedback loop control of pressure loss, which is based on the

relationship between the pressure and leakage rate, the control coefficient of temperature and current pulse, and the change law of temperature and pressure coupling. The temperature-current pulse control coefficient acts on the temperature heater to adjust the electric heating power by adjusting the pulse duty cycle.

4. Feasibility experiment verification and results

Based on the theoretical model of the temperature-pressure alternation of a coring device, in this study, a temperature-pressure coupling intelligent control system is designed and manufactured. Under the condition of ultrahigh pressure, the system should not only meet the requirements of ultrahigh pressure sealing and strength but also realize the controllable adjustment of pressure. To verify the feasibility and sealing stability of the control method, a temperature-pressure coupling test system is designed. The theory and system of temperature and pressure alternating control are verified by experiments.

As shown in Fig. 9, for the sake of test safety, the control object of the temperature-pressure alternating control system adopts an ultrahigh-pressure sealed cavity with an internal volume of 2 L, which truly simulates the ultrahigh-pressure liquid environment of the coring device (D.F. Wu et al., 2020). The temperature-pressure alternating control system relates to the cavity through threads, and the joint is sealed by ultrahigh pressure. The deep ultrahigh-pressure environment is simulated by the ultrahigh-pressure cycle failure detection system. At the same time, the flow leakage of the liquid chamber is detected. The power and temperature of the heater are controlled by an intelligent temperature controller, and the pressure change in the cabin is detected by a pressure gauge.

4.1. Test and calibration of the system leakage rate

Because of the high-pressure leakage and test error in the highpressure experimental liquid chamber, it is necessary to test the

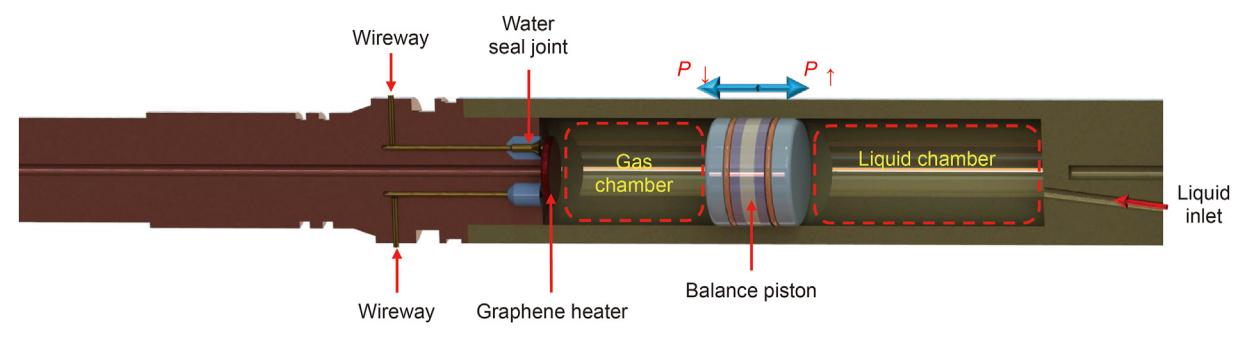


Fig. 7. Temperature-pressure coupling control system of the coring device.

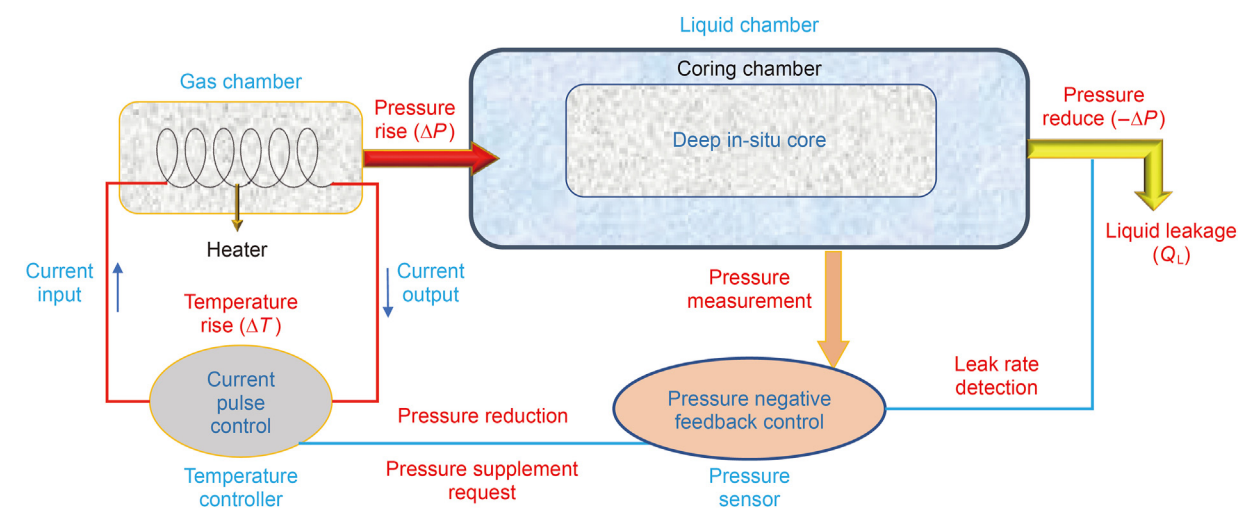


Fig. 8. Schematic diagram of the temperature-pressure coupling intelligent control system.

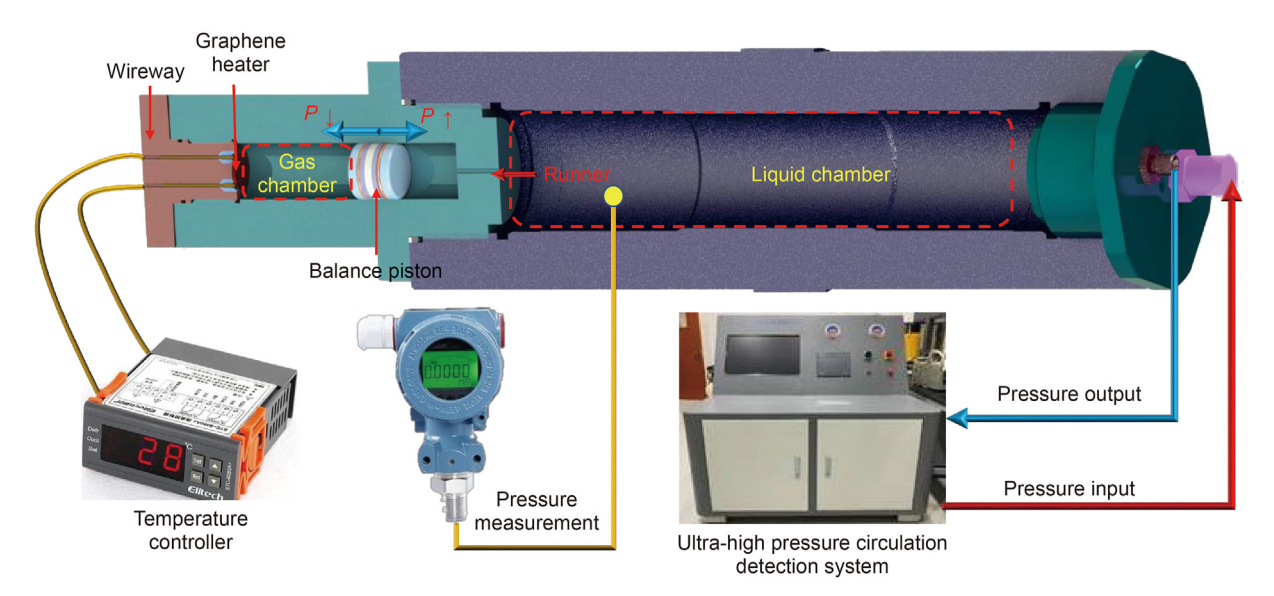


Fig. 9. Temperature-pressure coupling intelligent control test system.

pressure holding capacity of the high-voltage test cabin separately before testing the temperature-pressure coupling intelligent control system and calibrate the test accuracy of the system based on the test results.

A total of 10 groups of pressure holding experiments with different preset pressures were carried out. Because the pressure source is a high-pressure plunger pump, there is a certain deviation between the initial pressure and the set value. Ten groups of pressure values are set in ascending sequence from 15 MPa to 100 MPa, and the holding time is set from 0 to 0–150 s. The experimental temperature was 25 °C, and the pressure medium was water.

Figure 10a shows the pressure variation with time in a high-voltage test cabin under various pressures. The results show that after loading to the preset pressure, the pressure in the test chamber changes little with time, and the flatness of the whole preset value-time-pressure three-dimensional surface is good, which intuitively shows that the pressure in the test chamber is well maintained. Therefore, the system can be used as a test platform for the pressure keeping capability of the pressure keeping controller.

Figure 10b shows the variation in pressure leakage with time under various preset pressures, which can be used to calibrate the test accuracy of the high-voltage test system. According to the measured experimental results, the initial offset is set for the high-voltage test system, and the pressure value of the pressure keeping controller corresponding to the sealing time is corrected so that the measured pressure data are real data.

4.2. Experimental results and analysis

To verify whether the temperature-pressure coupling intelligent control system can work under deep pressure conditions, an ultrahigh-pressure test of 140 MPa was carried out, and the pressure was maintained for 30 min. To determine the pressure regulation ability of the intelligent temperature-pressure coupling control system, pressure control tests with initial pressures of 0 MPa (The pressure parameters in this paper are relative pressure), 1 MPa, 2 MPa, 5 MPa and 10 MPa were carried out for the sake of test safety. The test temperature ranged from room temperature (25 °C) to 300 °C, and the changes in pressure and temperature during the heating process were measured.

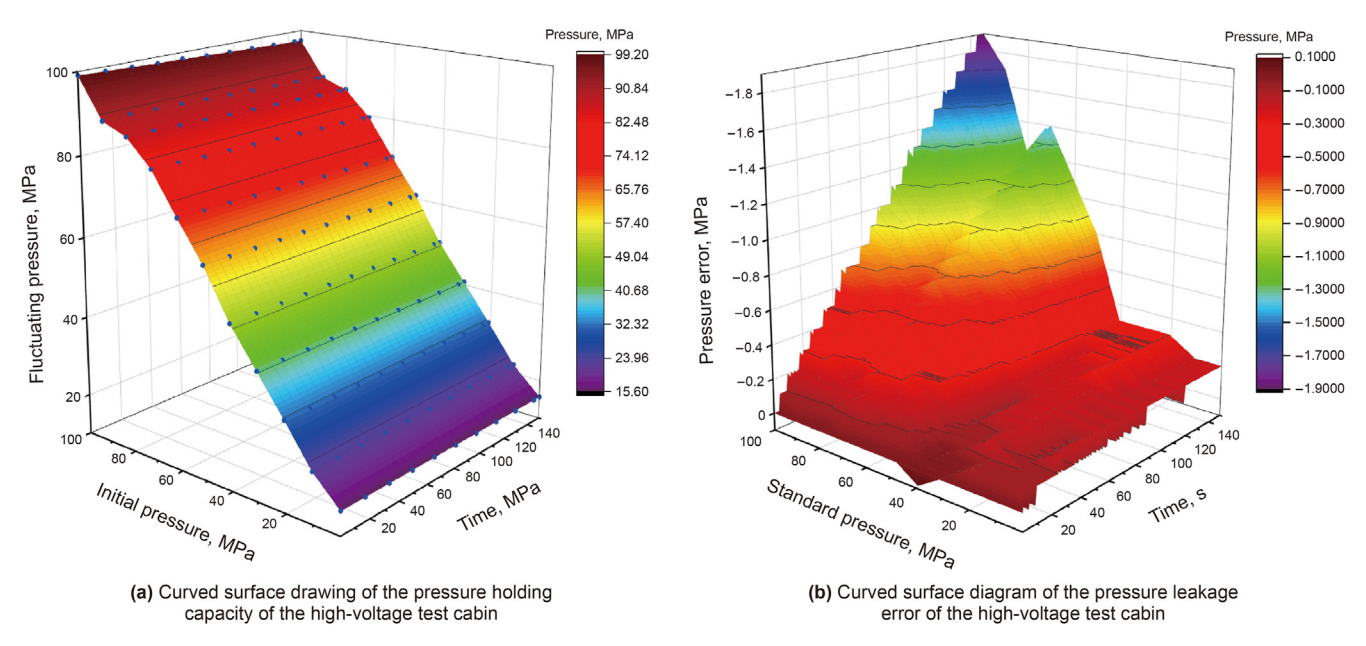


Fig. 10. Experimental results of pressure leak calibration in a high-voltage test cabin.

(1) Experimental verification of the ultrahigh-pressure seal

The test results are shown in Fig. 11a. The test lasted for 65 min, and the pressure was adjusted from atmospheric pressure to 140 MPa by the hydraulic control system. For safety reasons, the whole process cannot directly raise the pressure to the highest set pressure, so the pressure raising process was divided into four parts: 0–10 MPa, 10–30 MPa, 30–80 MPa and 80–140 MPa. When the pressure reached 140 MPa, the pressure remained stable. At the same time, leakage of the whole system was detected, as shown in Fig. 11b.

The test results show that the leakage rate of the high-pressure test is consistent with the initial calibrated leakage rate, and the leakage amount is caused by the ultrahigh-pressure test cabin. Therefore, it can be concluded that the intelligent temperature-pressure coupling control system can achieve stable sealing under every pressure condition and meet the strength requirements. When the pressure reached 140 MPa, long-term pressure sealing and system stability can be realized. The system can work stably in an ultrahigh environment.

(2) Temperature-pressure coupling alternating test

The initial pressure of the coring device directly determines the controllable range of the experiment. The initial gas pressure of this experiment was set to 0 MPa, 1 MPa, 2 MPa, 5 MPa and 10 MPa,

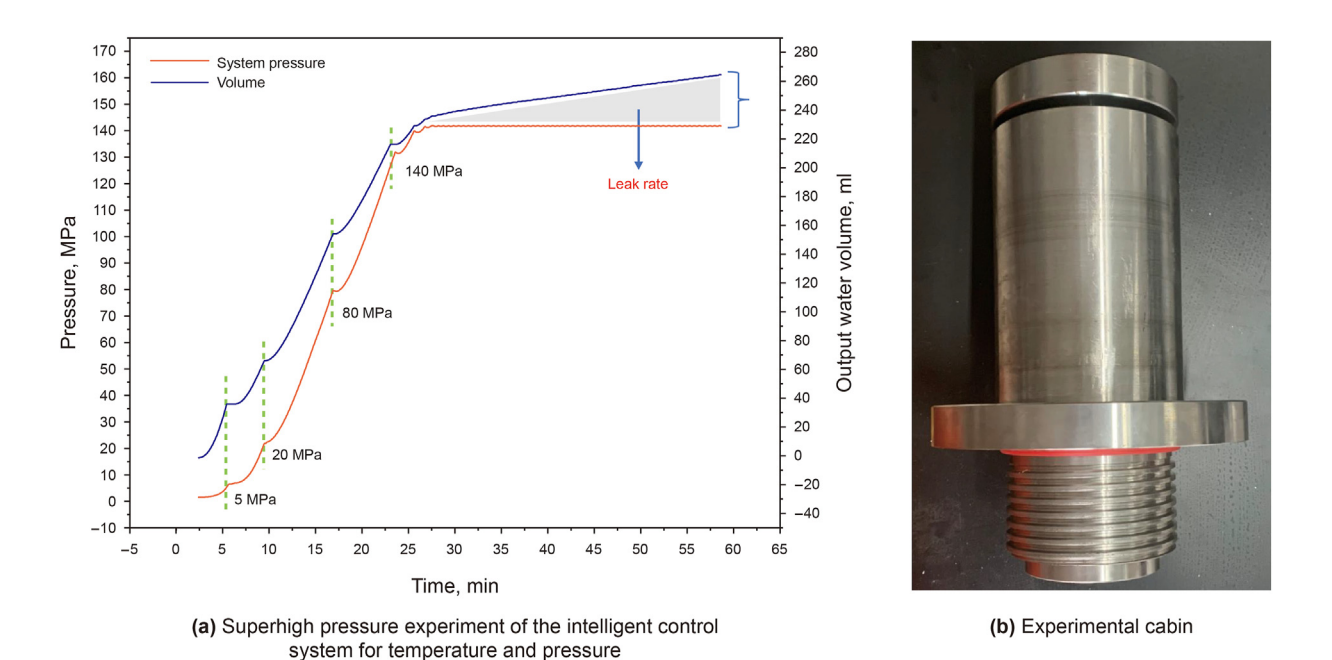


Fig. 11. Experimental curve and apparatus for ultrahigh-pressure experiments.

which was used to verify the feasibility of alternating the temperature and pressure control of the coring device and explore the influence of the initial pressure on the temperature and pressure curve. At the same time, it is considered that the balance piston may leak some liquid in the liquid-compatible cavity. The gas-liquid mixed state is formed in the gas-compatible cavity, so test 12.d was supplemented. In this experiment, 50% of the initial volume of the gas-compatible cavity was injected in advance, and the temperature-pressure coupling test was carried out under an initial pressure of 0 MPa.

Under initial pressure conditions of 0 MPa and 1 MPa, the curves of temperature and pressure are exponential. As shown in Fig. 12, when the initial pressure is 0 MPa, the maximum pressure that the system can control and compensate is 1.5 MPa. When the initial pressure is 1 MPa, the maximum pressure that the system can compensate is 2.3 MPa.

When the initial pressure of the system is above 2 MPa, the relationship between temperature and pressure is approximately linear, and its slope gradually increases with increasing initial pressure. As shown in Fig. 13, when the initial pressure is 2 MPa, the linear relationship between temperature and pressure is satisfied, and the slope of the fitting curve is 0.0048. When the initial pressure is 5 MPa, the slope is 0.016, and when the initial pressure is 10 MPa, the slope is 0.0342. It can be concluded that the influence of the initial pressure is very important in the temperature-pressure coupling alternating model.

Under the condition of prefilling with 50% water, it is found that the temperature-pressure alternating curve is quite different from that of a pure gas environment. The maximum pressure compensation range is 40.3 MPa, far exceeding the pressure compensation amount of pure gas. When the pressure reaches 17 MPa and the temperature reaches 645 K, the temperature-pressure alternating curve returns to a linear relationship. Therefore, the test results show that the pressure can be better controlled by changing the initial volume ratio of liquid to gas. The purpose of this investigation is to study the temperature-pressure alternating model and verify its feasibility. No further research has been done on the specific influence of the gas-liquid volume ratio, and this topic will be studied in subsequent work.

The slope of the temperature-pressure alternating curve at low pressure (<1 MPa) changes. Through the temperature-pressure test of 50% volume water, it is found that the change may be caused by the water component in the gas, which will be studied later.

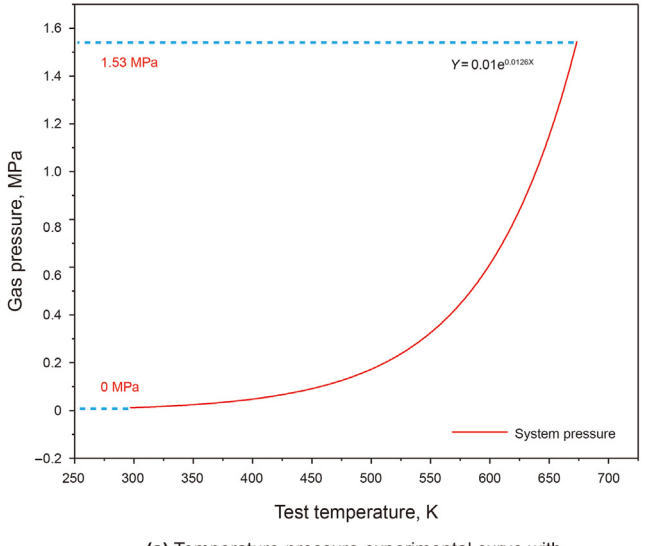
When the pressure is greater than 2 MPa, the test curve of the temperature-pressure alternation agrees with the theoretical derivation in advance, which proves the correctness of the theory and verifies the pressure compensation ability of the intelligent compensation system of the temperature-pressure alternation.

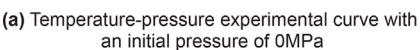
In order to further verify the compensation effect of temperature on pressure under higher pressure conditions, pressure compensation experiments with an initial temperature of 50 °C and an initial temperature of 70 °C were carried out, and the pressure medium was replaced with water to raise the temperature to 150 °C respectively. As shown in Figs. 14 and 15, the pressure inside the pressure device increased linearly with the increase of temperature, and the final pressure was even 150 MPa, which fully explained that, Under the condition of using water as pressure medium, the device has higher pressure compensation effect.

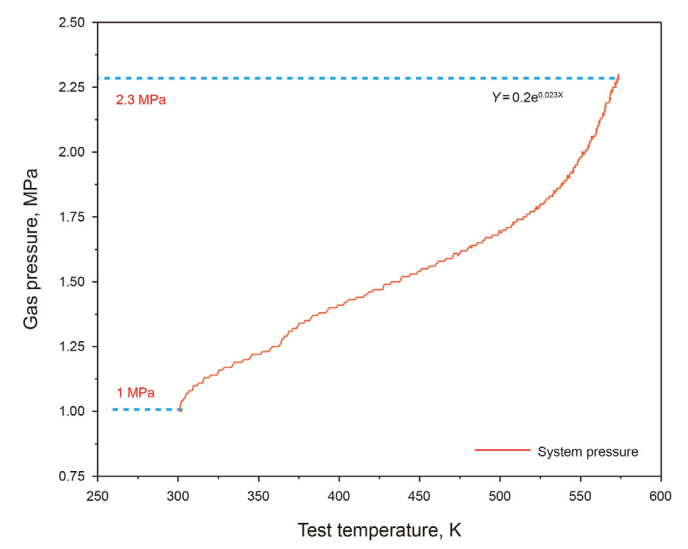
Through the above tests, it can be concluded that the ultrahighpressure seal and stability of the intelligent compensation system with alternating temperature and pressure can meet the needs of deep coring pressure environments, and the pressure of the compensation system can be effectively controlled by the alternating temperature and pressure control system.

4.3. Research on pressure control algorithm of temperaturepressure coupling system

The core of temperature-pressure coupling control system is the mathematical model and control algorithm. In this paper, the thermal fluid-solid coupling dynamic model of the pressure control system was established, as shown in Fig. 16a. The solid piston contacts the liquid domain and the gas domain respectively, and the fluid pressure acted on the piston. The gas domain was a non-isothermal flow system under the condition of temperature-pressure field. The gas domain was set as a compressible fluid. The constitutive equation of the gas domain is:







(b) Temperature-pressure experimental curve with an initial pressure of 1MPa

Fig. 12. Coupling curve of temperature-pressure at a lower initial pressure (<2 MPa).

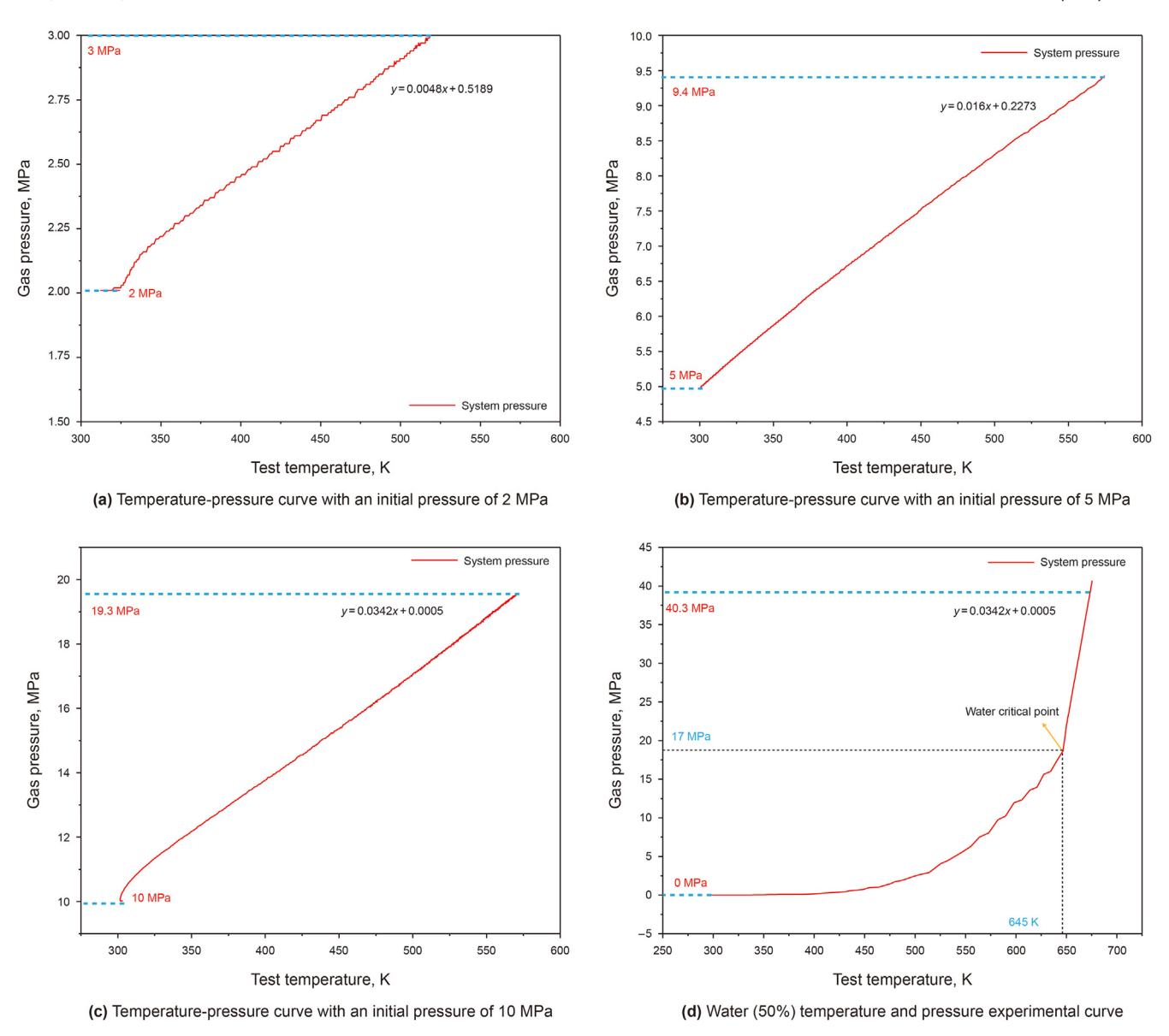


Fig. 13. Coupling curve of temperature-pressure at a higher initial pressure (>1 MPa).

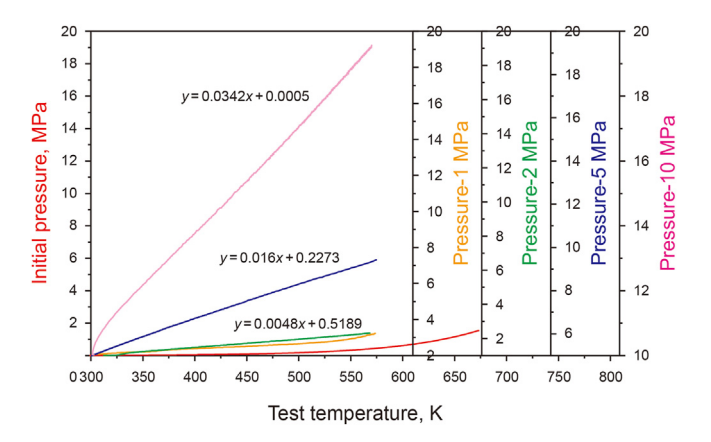


Fig. 14. Experimental temperature-pressure curves for 0–10 MPa pressure gradients.

$$\rho_{air} \left(\frac{\partial \mathbf{v}_{air}}{\partial t} + \mathbf{v}_{air} \bullet \nabla \mathbf{v}_{air} \right) = -\nabla p_{air} + \nabla \\
\bullet \left(\mu_{air} \left(\nabla \mathbf{v}_{air} + (\nabla \mathbf{v}_{air})^T \right) - \frac{2}{3} \mu_{air} (\nabla \bullet \mathbf{v}_{air}) I \right) + F$$
(25)

Where, v_{air} was the fluid velocity, p_{air} was the fluid pressure, ρ_{air} was the fluid density, μ_{air} was the hydrodynamic viscosity. In the Formula.25, the corresponding relationship of each physical item was as follows:

Inertia force F_i satisfied:

$$F_{i} = \rho_{air} \left(\frac{\partial v_{air}}{\partial t} + v_{air} \bullet \nabla v_{air} \right)$$
 (26)

Fluid pressure F_{air} satisfied:

$$F_{air} = -\nabla p_{air} \tag{27}$$

Viscous force F_V satisfied:

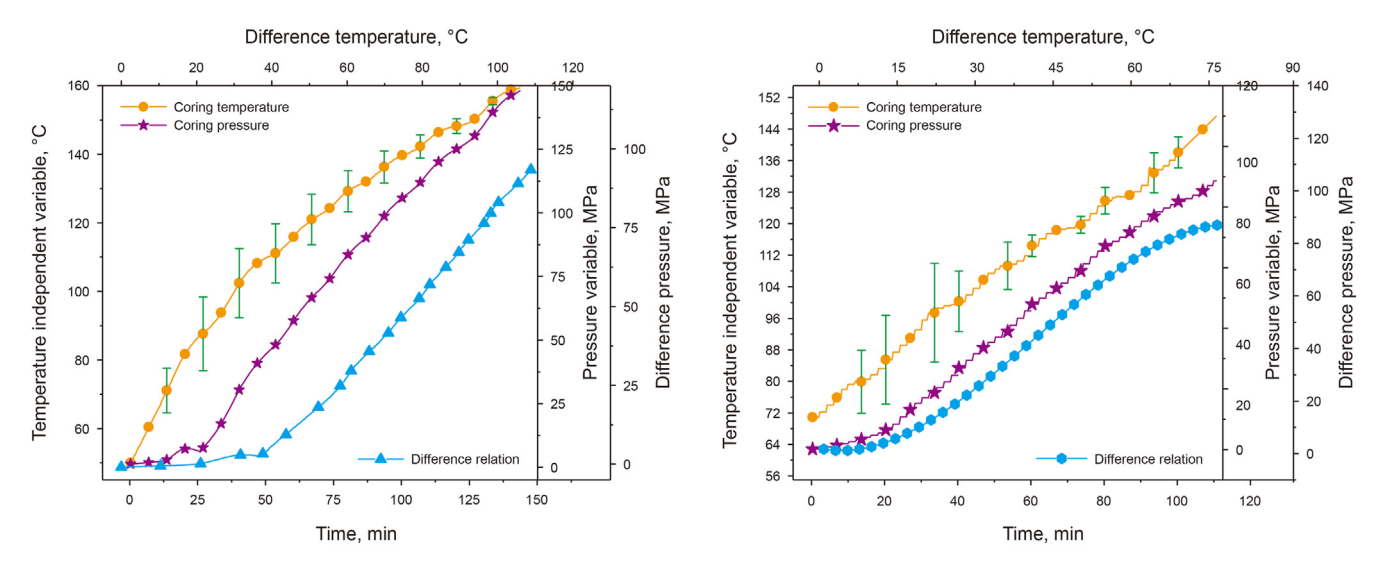


Fig. 15. Temperature-pressure coupling control curve of pressure control device.

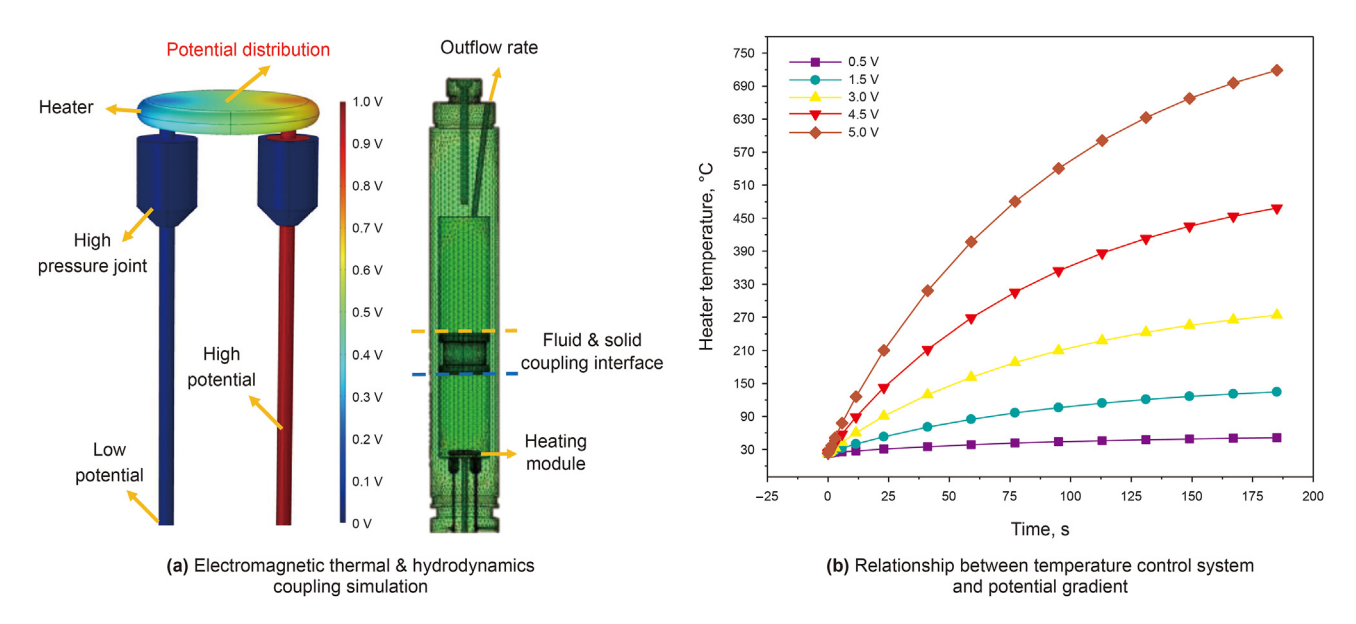


Fig. 16. Numerical simulation experiment of temperature-pressure coupling system.

$$F_{V} = \nabla \bullet \left(\mu_{air} \left(\nabla v_{air} + \left(\nabla v_{air} \right)^{T} \right) - \frac{2}{3} \mu_{air} (\nabla \bullet v_{air}) I \right)$$
 (28)

Based on Formula.25, ignoring the weight of the piston, the relationship between the temperature of the gas domain and the pressure of the non-isothermal flow system can be obtained.

The electromagnetic thermal field of the heating system is calculated, and the result was shown in Fig. 16a. For the calculation of the control system, both voltage and pulse control can adjust the power of the heater. But voltage control has the advantage of simple calculation. Therefore, voltage control is selected in this model. The low potential terminal of the heating system is 0 V, and the high potential terminal is used as the input control quantity of the control system. The potential distribution diagram shows that the difference of the heating system is concentrated at both ends of the heater, so its electromagnetic heat is concentrated in the heater.

The numerical simulation was based on the deep pressure leakage simulation model, and its control algorithm was based on

negative feedback PID. In the process of numerical simulation, the real-time pressure in the ballast tank is transformed into the control output voltage, so the result can basically reflect the control results under the real working conditions, and has a certain reliability.

At the same time, the overall electromagnetic temperature-pressure simulation calculation was carried out to obtain the relationship between the heater temperature and the potential input, as shown in Fig. 16b. The potential value varies in a gradient from 1 V to 5 V. The temperature of the heater rises exponentially due to the heat exchange between the heater and the gas domain. The differential equation of heat conduction is:

$$\rho_{air}c_{air}\frac{\partial t}{\partial \tau} = \left[\frac{\partial}{\partial x}\left(\lambda\frac{\partial t}{\partial x}\right) + \frac{\partial}{\partial y}\left(\lambda\frac{\partial t}{\partial y}\right) + \frac{\partial}{\partial z}\left(\lambda\frac{\partial t}{\partial z}\right)\right] + q_V \tag{29}$$

In the same time range, the final temperature of the heater increases with the increase of voltage.

Due to the control system involves many physical fields, the

control function has great uncertainty, so it is impossible to use a fixed control algorithm. Therefore, this paper adopted a three term PID control algorithm based on the optimal cardinality. The optimal cardinality of the whole system model was selected to obtain the control input variable cardinality with the minimum transient error value. The Formula is expressed as:

$$P_{control} = F(V_{\mathbf{R}}) + e_{min} \tag{30}$$

Set the initial pressure of the pressure control system as 1 MPa, and set the uniform fluid leakage rate $L_{\it w}=5ml/s$ at the liquid outlet. In order to obtain the optimal cardinality, set the gradient voltage input to obtain the system pressure curve, as shown in Fig. 17.

In Fig. 17, when the voltage is 0V and there is no heating system, the pressure decreased linearly. The curve was used as the basic comparison curve of the control system. When the potential gradually increases, the pressure curve gradually curls upward. Meanwhile, the pressure reduction rate decreases gradually. When the pressure is greater than 3V, the pressure tends to rise, and the rising rate increases gradually. Pressure drop and rise are not allowed in coring environment. Therefore, the optimal voltage cardinal is finally selected as 3V.

On this basis, the negative feedback control algorithm is introduced, and the transient control pressure is taken as the control input of the control system to obtain the transient proportional self-gain control algorithm:

$$V_{h-t1} = V_{\mathbf{B}} + k_{pi}G_{j}(P_{t0} - P_{initial})V_{\mathbf{B}}$$
(31)

Where V_{h-t1} represents the transient input voltage control parameter; k_{pi} is the proportional self-gain coefficient; P_{t0} represents the pressure value at the previous moment; $P_{initial}$ is the pressure control value; G_j is a negative magnitude coefficient automatically adjusted according to the magnitude of the pressure control magnitude.

For the pressure control system, the optimal proportional selfgain coefficient is not clear. Therefore, through the gradient experiment, the convergence of the transient proportional self-gain control algorithm and the optimal self-gain coefficient are verified.

As shown in Fig. 18, sets of proportional coefficients are set from 0 to 5, and the proportional self-gain control algorithm is used as the control equation of the input voltage to obtain the pressure

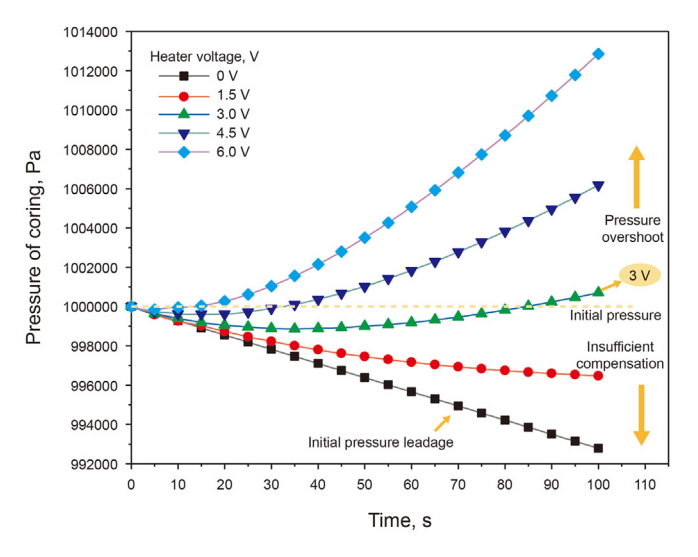


Fig. 17. Relationship between potential and pressure under uniform leakage at 1 MPa pressure.

curve of the system. In the Fig. 18, the pressure have a certain initial leakage, and the rate gradually decrease, then gradually increase, and fall back at the highest point. Under the control of voltage, the pressure of the whole system oscillates back and forth in the attachment of the initial pressure line and gradually converges. With the increase of scale coefficient, the maximum error of the system decreases and the regression distance decreases. The stability of negative feedback proportional control system is also gradually enhanced.

Although the negative feedback proportional control was introduced, the feedback error of pressure was always based on the previous pressure state, so there was always a certain steady-state error in the control system. Fig. 19 shows the pressure error after the pressure system finally converges completely under the conditions of different scale coefficients. At this time, the pressure leakage and compensation of the system have tended to balance, but did not return to the initial pressure. With the increase of the proportional coefficient, the steady-state error gradually decreases. In k_{p6} , the system error reaches a minimum of 250 Pa.

To make the system converge further, the control algorithm introduced the first-order integral and first-order differential terms of the pressure error time variation function. The steady-state error is further reduced by calculating the accumulated error. The control algorithm is as follows:

$$V_{h-t1} = V_{\mathbf{B}} + k_{pi}G_{j}(P_{t0} - P_{initial})V_{\mathbf{B}} + k_{li}G_{i}V_{\mathbf{B}} \int t_{0}e(\Delta P_{t0})dt + k_{Di}G_{d}V_{\mathbf{B}}de(\Delta P_{t0})dt$$

$$(32)$$

Where, G_i is the negative order parameter of the integral term, G_d is the negative order coefficient of the differential term, ΔP_{t0} is the transient pressure error, k_{li} is the integral coefficient, k_{Di} is the differential coefficient.

Set different differential coefficient and integral parameter ratio respectively from V_1 to V_5 . Obtain different pressure system control curves. As shown in Fig. 20, under the control of the optimal cardinal three term PID algorithm, the pressure system gradually tends to the initial value under short oscillation. Its steady-state error is smaller than that of the simple proportional self-gain control algorithm. In the control time of 500 s, the final pressure control accuracy reached 20 Pa. This also verifies the feasibility of the control system and the stability of the control algorithm.

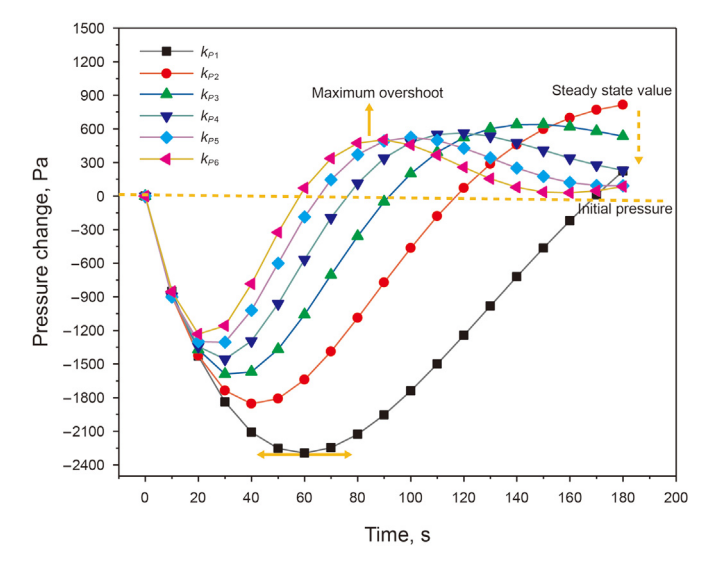


Fig. 18. Pressure control curve based on optimal cardinality negative feedback proportional control algorithm.

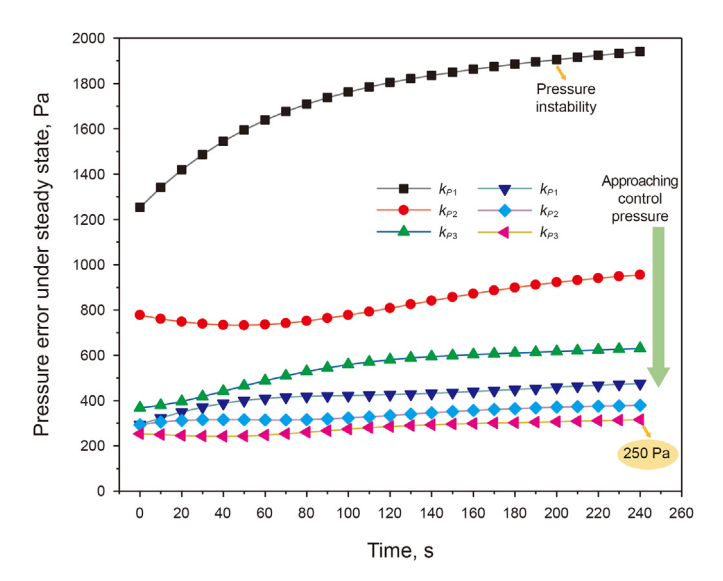


Fig. 19. Steady state control error curve of optimal cardinality negative feedback proportional control algorithm.

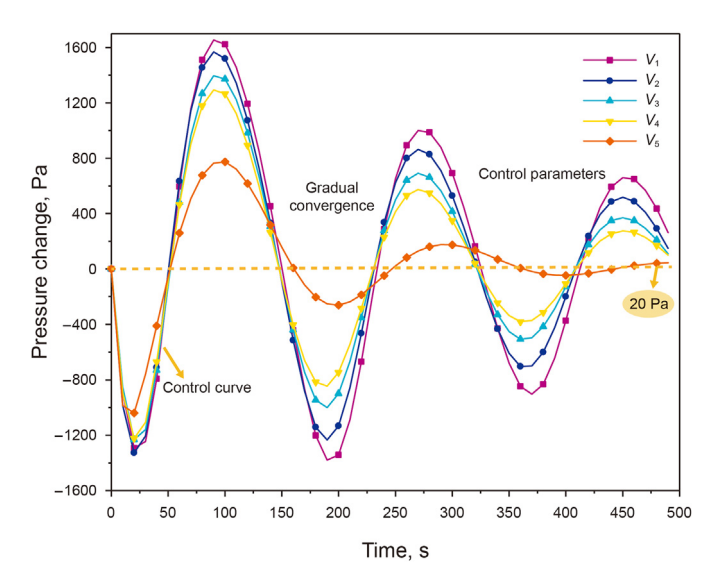


Fig. 20. Pressure control curve of optimal cardinality three term PID algorithm.

5. Conclusion

The temperature-pressure coupling alternating theory in ICP-Coring is constructed in this paper. An intelligent control system for the temperature and pressure of the coring device is developed and verified by experiments. The optimality cardinal three term PID algorithm is proposed and the numerical simulation experiment of pressure control system is carried out. The test results show that:

- (1) The ultrahigh-pressure seal and stability of the intelligent compensation system with alternating temperature and pressure can meet the needs of a deep coring pressure environment. The maximum pressure-bearing capacity of the whole system reaches 140 MPa and the effective pressure compensation range is 20 MPa.
- (2) The temperature-pressure alternating control system can effectively control the pressure of the system. The experimental results show that the pressure increment curves are

- different under different initial pressure conditions. With the increase of initial pressure, the pressure increases rate increases.
- (3) The optimality cardinal three term PID algorithm is used to control the voltage input, and the intelligent control of pressure is realized. The optimal cardinality 3 V in the system is obtained. When only proportional self-gain control is used, the minimum steady-state error is 200 Pa. When three term PID algorithm is adopted, the steady-state error is reduced to 20 Pa. The control accuracy of the whole pressure control system reaches 0.1%.

Using the relationship between gas temperature and pressure, a high-precision pressure control system suitable for small space is innovatively developed, and the pressure control range is large. This paper provides a method for pressure control of ICP-Coring under ultrahigh pressure and confined spaces and then verifies it. In future work, the accurate control algorithm of pressure under different initial conditions will be further studied.

Data availability

The raw/processed data used to support the findings of this study have not been made available because the data also forms part of an ongoing study.

Declaration of competing interest

The authors declare that they have no known competing financial interests or personal relationships that could have appeared to influence the work reported in this paper.

Acknowledgments

This work was supported by the National Natural Science Foundation of China (grant numbers 51827901, 51805340). The financial aids are gratefully acknowledged. This project was also funded by the Program for Guangdong Introducing Innovative and Enterpreneurial Teams (No. 2019ZT08G315) and Shenzhen Basic Research Program (General Program) (No. JCYJ20190808153416970).

References

Alali, A.M., Abughaban, M.F., Aman, B.M., et al., 2021. Hybrid data driven drilling and rate of penetration optimization. J. Petrol. Sci. Eng. 200. https://doi.org/10.1016/ i.petrol.2020.108075.

Ciannella, S., Damasceno, A.S., Nunes, Í.C., et al., 2018. Using hot-vapor bypass for pressure control in distillation columns. Chin. J. Chem. Eng. 26 (1), 144–151. https://doi.org/10.1016/j.cjche.2017.07.023.

Dickens, G.R., Wallace, P.J., Paull, C.K., et al., 2000. Detection of methane gas hydrate in the pressure core sampler (PCS). volume-pressure-time relations during controlled degassing experiments 164, 113–126. https://doi.org/10.2973/odp.-proc.sr.164.210.2000. Texas A & M University College Station Tx.

Ding, J.W., Wan, X., Hong, Z.S., et al., 2021. Excess pore water pressure induced by installation of precast piles in soft clay. Int. J. GeoMech. 21 (9). https://doi.org/ 10.1061/(ASCE)GM.1943-5622.0001992.

Gao, M.Z., Zhang, Z.L., Yin, X.G., et al., 2018a. The location optimum and permeability enhancing effect of a low-level shield rock roadway. Rock Mech. Rock Eng. 51 (9), 2935—2948. https://doi.org/10.1007/s00603-018-1461-x.

Gao, M.Z., Zhang, R., Xie, J., et al., 2018b. Field experiments on fracture evolution and correlations between connectivity and abutment pressure under top coal caving conditions. Int. J. Rock Mech. Min. Sci. 111, 84–93. https://doi.org/10.1016/ j.ijrmms.2018.01.003.

Gao, M.Z., Zhang, S., Li, J., et al., 2019. The dynamic failure mechanism of coal and gas outbursts and response mechanism of support structure. Therm. Sci. 23 (3), 867–975. https://doi.org/10.2298/TSCI180610122G.

Gao, M.Z., Liu, J.J., Lin, W.M., et al., 2020. Study on in-situ stress evolution law of ultra-thick coal seam in advance mining. Coal Sci. Technol. 48 (2), 28–35 (in Chinese)

Gao, M.Z., Xie, J., Gao, Y.N., et al., 2021. Mechanical behavior of coal under different

mining rates: a case study from laboratory experiments to field testing. Int. J. Min. Sci. Technol. 31 (5), 825–841. https://doi.org/10.1016/j.ijmst.2021.06.007.

- Gao, M.Z., Chen, L., Fan, D., Yang, M.Q., et al., 2021. Principle and technology of coring with in-situ pressure and gas maintaining in deep coal mine. J. China Coal Soc, 46 (3), 885–897 (in Chinese).
- Gao, M.Z., Xie, J., Guo, J., et al., 2021. Fractal evolution and connectivity characteristics of mining-induced crack networks in coal masses at different depths. Geomechanics and Geophysics for Geo-Energy and Geo-Resources 7 (1). https://doi.org/10.1007/s40948-020-00207-4.
- Gao, M.Z., Hao, H.C., Xue, S.N., et al., 2021. Discing behavior and mechanism of cores extracted from Songke-2 well at depths below 4,500 m. Int. J. Rock Mech. Min. Sci. 149. https://doi.org/10.1016/j.ijrmms.2021.104976.
- Gao, M.Z., Wang, M.Y., Xie, J., et al., 2021. Experimental study on the mechanical response mechanism of different unloading rate to coal rock mechanics. Advanced Engineering Sciences 53 (6), 54–63 (in Chinese.
- Gao, M.Z., Yang, B.G., Xie, J., et al., 2022. The mechanism of microwave rock breaking and its potential application to rock-breaking technology in drilling. Petrol. Sci. 19 (3), 1110–1124. https://doi.org/10.1016/j.petsci.2021.12.031.
- Guan, W., Wang, X.Y., Zhao, H., et al., 2021. Exploring the high load potential of diesel—methanol dual-fuel operation with Miller cycle, exhaust gas recirculation, and intake air cooling on a heavy-duty diesel engine. Int. J. Engine Res. 22 (7). https://doi.org/10.1177/1468087420926775.
- Li, C.S., W, X., Q, H.B., et al., 2020. Pressure performance improvement by dual-mode control in digital pump/motor. J. Cent. S. Univ. 27 (9), 2628–2642. https:// doi.org/10.1007/s11771-020-4487-7.
- Lyras, T., Karathanassis, I.K., Kyriazis, N., et al., 2021. Modelling of liquid oxygen nozzle flows under subcritical and supercritical pressure conditions. Int. J. Heat Mass Tran. 177. https://doi.org/10.1016/j.ijheatmasstransfer.2021.121559.
- Lyu, Y.F., Hu, X.L., Jin, F.M., et al., 2021. Quantitative evaluation of lateral sealing of extensional fault by an integral mathematical-geological model. Petrol. Explor. Dev. 48 (3), 569–580 https://doi.org/10.1016/S1876-3804(21)60046-0.
- Milkov, A.V., Dickens, G.R., Claypool, G.E., et al., 2004. Co-existence of gas hydrate, free gas, and brine within the regional gas hydrate stability zone at Hydrate Ridge (Oregon margin). evidence from prolonged degassing of a pressurized core. Earth & Planetary Science Letters 222 (3–4), 829–843. 10.1016/j.epsl. 2004.03.028.
- Pang, X.Q., Jia, C.Z., Wang, W.Y., 2015. Petroleum geology features and research developments of hydrocarbon accumulation in deep petroliferous basins. Petrol. Sci. 12, 1–53. https://doi.org/10.1007/s12182-015-0014-0.
- Pruchnicki, E., Chen, X.Y., Dai, H.H., 2021. New refined model for curved linear anisotropic rods with circular cross section. In: Applications in Engineering Science, vol. 6. https://doi.org/10.1016/J.APPLES.2021.100046.
- Ruffine, L., Deusner, C., Haeckel, M., et al., 2021. Effects of postglacial seawater intrusion on sediment geochemical characteristics in the Romanian sector of the Black Sea. Mar. Petrol. Geol. 123. https://doi.org/10.1016/

- j.marpetgeo.2020.104746.
- Takigawa, T., Horinaka, J., 2020. Application of a clapeyron-type equation to the volume phase transition of polymer gels, 6(3). https://doi.org/10.3390/ gels6030025.
- Tian, C., Wei, X.W., Yang, C., et al., 2021. Optimization technology of frequency conversion constant pressure control system of mine emulsion pump station in electrical engineering and automation specialty. Adv. Civ. Eng. https://doi.org/ 10.1155/2021/5569994, 2021.
- Wu, N.H., Xie, H.P., Chen, L., et al., 2020. Sealing form and failure mechanism of deep in-situ rock core pressure-maintaining controller. Geofluids. https://doi.org/ 10.1155/2020/8892720, 2020.
- Wu, D.F., Guan, Z.W., Cheng, Q., et al., 2020. Development of a friction test apparatus for simulating the ultra-high pressure environment of the deep ocean. Wear 452–453. https://doi.org/10.1016/j.wear.2020.203294, 2020.
- Xiang, Z., Zhang, N., Xie, Z.Z., et al., 2021. Cooperative control mechanism of long flexible bolts and blasting pressure relief in hard roof roadways of extra-thick coal seams: a case study. Appl. Sci. 11 (9). https://doi.org/10.3390/app11094125.
- Xie, H.P., 2017. Research framework and anticipated results of deep rock mechanics and mining theory. Advanced Engineering Sciences 49 (2), 1–16 (in Chinese).
- Xie, H.P., 2019. Research review of the state key research development program of China deep rock mechanics and mining theory. J. China Coal Soc. 44 (5), 1283–1305 (in Chinese).
- Xie, H.P., Gao, F., Ju, Y., 2015. Research and development of rock mechanics in deep ground engineering. Chin. J. Rock Mech. Eng. 34 (11), 2161–2178 (in Chinese).
- Yang, J., Liu, C.H., Liu, H.B., et al., 2007. Strength and stability analysis of deep sea drilling risers. Petrol. Eng. 4, 60–65. https://doi.org/10.1007/BF03187443.
- Yang, G., Du, J.M., Fu, X.Y., et al., 2017. Asymmetric fuzzy control of a positive and negative pneumatic pressure servo system. Chin. J. Mech. Eng. 30, 1438—1446. https://doi.org/10.1007/s10033-017-0194-1.
- Yang, H.Q., Zhang, N., Han, C.L., et al., 2021. Stability control of deep coal roadway under the pressure relief effect of adjacent roadway with large deformation: a case study. Sustainability 13 (8). https://doi.org/10.3390/SU13084412.
- Zhang, J., Yang, R.S., 2009. Research on Mechanics Properties of the Deep Brittle Rock with Triaxial Unloading Experiment. China Mining Magazine (in Chinese).
- Zhang, R.Y., Li, J., Liu, G.H., et al., 2021. The coupled model of wellbore temperature and pressure for variable gradient drilling in deep water based on dynamic mass flow. J. Petrol. Sci. Eng. 205. https://doi.org/10.1016/J.PETROL.2021.108739.
- Zhu, Z.D., Pu, S.Y., Zhang, J.H., et al., 2021. Water resistance and compressibility of silt solidified with lime and fly-ash mixtures. Environ. Earth Sci. https://doi.org/ 10.1007/S12665-021-09398-9.